NANO LETTERS

Letter

pubs.acs.org/NanoLett

Nanoscale Spatial Coherent Control over the Modal Excitation of a Coupled Plasmonic Resonator System

Toon Coenen,[†] David T. Schoen,[‡] Sander A. Mann,[†] Said R. K. Rodriguez,[†,§,⊥] Benjamin J. M. Brenny,[†] Albert Polman,[†] and Mark L. Brongersma*[,‡]

[†]Center for Nanophotonics, FOM Institute AMOLF, Science Park 104, 1098 XG Amsterdam, The Netherlands

[‡]Geballe Laboratory for Advanced Materials, Stanford University, Stanford, California 94305, United States

[§]Philips Research Laboratories, High Tech Campus 4, 5656 AE Eindhoven, The Netherlands

Supporting Information

ABSTRACT: We demonstrate coherent control over the optical response of a coupled plasmonic resonator by high-energy electron beam excitation. We spatially control the position of an electron beam on a gold dolmen and record the cathodoluminescence and electron energy loss spectra. By selective coherent excitation of the dolmen elements in the near field, we are able to manipulate modal amplitudes of bonding and antibonding eigenmodes. We employ a combination of CL and EELS to gain detailed insight in the power dissipation of these modes at the nanoscale as CL selectively probes the radiative response and EELS probes the combined effect of Ohmic dissipation and radiation.

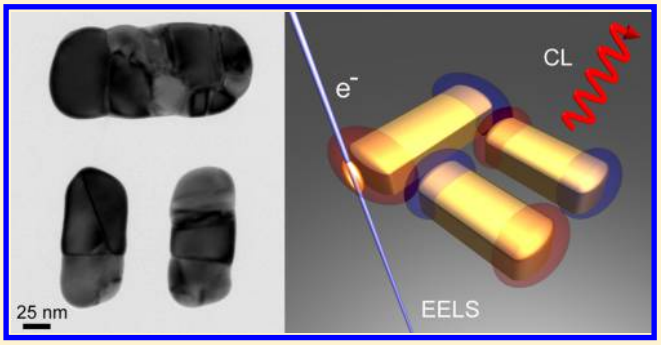

KEYWORDS: *Plasmonics, coherent control, metamolecules, cathodoluminescence spectroscopy, electron energy loss spectroscopy, near-field coupling*

Localized surface plasmons, the optical-frequency resonant modes of unbound electrons in metal nanoparticles, provide a unique way to control light−matter interaction at the nanoscale. The surface plasmon resonance frequency of a nanoparticle is determined by the density of free carriers in the metal, its geometry, and its dielectric environment. The interaction of light with plasmonic structures can be tailored even further when plasmonic elements are coupled. When particles are placed in each other's near-field, modal hybridization occurs, leading to plasmonic "bonding" and "antibonding" modes.[1] Such plasmonic coupling is enabled by the near-field overlap of the resonant modes. The coherent interaction between the coupled plasmonic modes can lead to strongly directional emission into the far-field.[2,3] Further control over the resonant spectra, near-fields, and angular scattering distributions can be achieved when resonant modes of different nature interact. For example, the interference between a high quality factor (high-Q) subradiant mode and a low-Q superradiant mode, can lead to a dispersive Fano line shape or plasmon-induced transparency (PIT) window where low extinction goes hand in hand with locally enhanced near-fields.[4−17] Coupling resonant plasmonic systems thus provides a unique way to control how light is absorbed and scattered and how the optical near-field is distributed over space.

However, the functionality and optical response of a plasmonic nanostructure is not only determined by its geometry but also by the way it is excited. There have been efforts to coherently control the amplitude and phase of near-fields in plasmonic structures by structuring conventional far-field illumination in the temporal and spatial domain. In the case of temporal control, appropriately shaped femtosecond laserpulses are used that directly influence the plasmon dynamics on the relevant time scale.[18,19] Spatial wavefront shaping has also been used as an alternative method for coherent control.[20] In such experiments the polarization of the incoming field(s) provides yet another degree of freedom.[21,22] However, most of these approaches are still limited in resolution by diffraction, and as a result, it is not possible to individually excite the constituent elements of the resonant system. This severely limits to what extent the modal interaction can be studied and controlled, as the plasmonic interaction occurs on length scales as small as 10 nm.

As an alternative to optical excitation, we use a tightly focused electron beam as a local coherent excitation source. A fast electron traversing a polarizable medium provides a very "pure" source of optical excitation in which the time-varying electric field about each electron's trajectory couples to the resonant eigenmodes' electric field distribution in the direction of the beam. The excitation resolution is determined by the electron beam waist and the extent of the evanescent field,

Received: September 8, 2015
Revised: October 8, 2015

 © XXXX American Chemical Society

DOI: 10.1021/acs.nanolett.5b03614
Nano Lett. XXXX, XXX, XXX−XXX

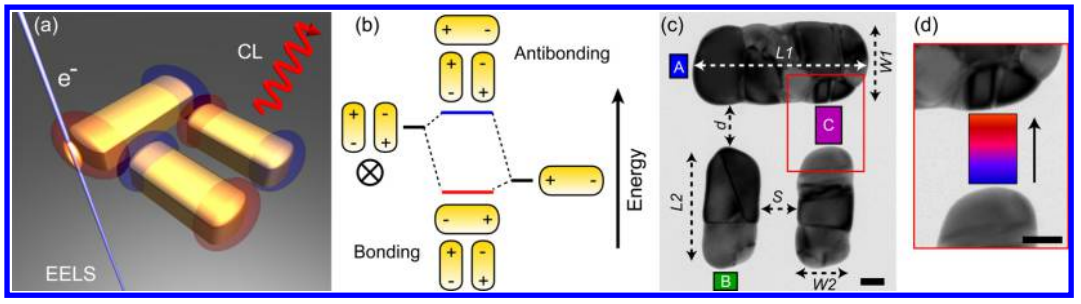

Figure 1. (a) Plasmonic dolmen structure composed of a resonantly coupled monomer and dimer is excited using high-energy electrons. CL and EELS spectra are measured as an electron beam is scanned over the surface. (b) Hybridization scheme for the dolmen. The subradiant antisymmetric dimer mode hybridizes with the superradiant dipolar momomer mode giving rise to a low-energy bonding mode and a high-energy antibonding mode. The ⊗ symbol indicates that a mode is symmetry forbidden for plane-wave excitation at normal incidence. (c) Bright-field TEM image of a gold dolmen structure studied with EELS and CL; size parameters are indicated. The blue (A), green (B), and magenta boxes (C) indicate excitation areas that are investigated in detail. The red box corresponds to the image field in (d). Scale bars: 25 nm.

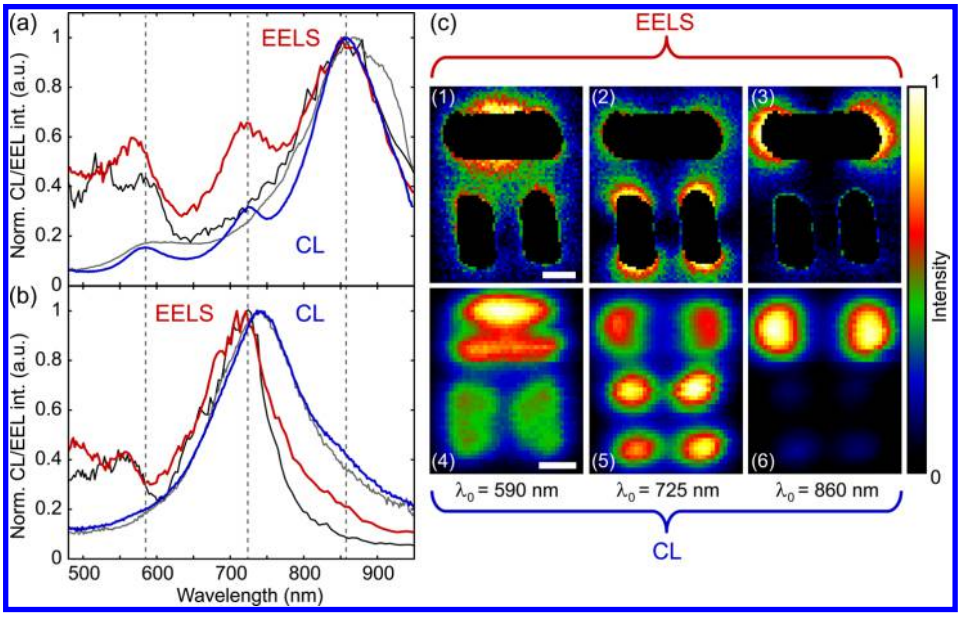

Figure 2. (a) CL (blue) and EELS (red) spectrum for excitation of the dolmen at position A as shown in Figure 1c, directly driving the monomer. CL (gray curve) and EELS (black curve) measurements taken at position A on an isolated monomer are shown for reference. (b) CL and EELS spectrum for excitation position B where we directly drive one of the dimer rods. Again, CL (gray curve) and EELS (black curve) measurements taken at position B on an isolated dimer are shown for reference (c) 2D EELS (images 1−3) and CL (images 4−6) for λ_0 = 590, 725, and 860 nm, respectively, integrated over a 30 nm bandwidth. Scale bars: 50 nm.

which is typically 10−20 nm. Electrons can be used to efficiently excite local electromagnetic modes with symmetric charge distributions such as vertical dipole or linear quadrupole modes, which are inaccessible to light under normal incidence. Furthermore, electrons can directly excite guided modes below the light line in vacuum such as surface plasmon polariton modes, which are momentum forbidden for light. The coupling between the electrons and the polarizable medium is probed by studying the light emission (cathodoluminescence (CL) spectroscopy[12,23−27]) or the energy-loss experienced by the electrons (electron energy-loss spectroscopy (EELS)[28−33]). CL and EELS provide complementary information, as CL selectively probes the radiative response, whereas EELS probes the combined effect of Ohmic dissipation and radiation.[34−38]

In this Letter, we use an electron beam to coherently control and probe an elemental coupled plasmonic system at a deep-subwavelength scale. In particular, we perform EELS and CL spectroscopy on the well-known plasmonic "dolmen" structure in which a single plasmonic nanorod is capacitively coupled to an orthogonally oriented dimer that is composed of two parallel coupled nanorods (Figure 1a).[4−6,39−43] The monomer rod supports a superradiant dipole resonance that couples to a subradiant resonance with an antisymmetric field distribution in the dimer. The two "bare states" hybridize into a low-energy bonding mode and high-energy antibonding mode (Figure 1b). We demonstrate that the electron beam excitation method provides an alternative pathway to coherent control in plasmonics and can be employed to tailor the local field distributions, which in turn directly influence light emission and absorption processes in the structure.

Gold dolmens were fabricated on 15 nm thick Si_3N_4 membranes using a combination of electron beam lithography (EBL), thermal evaporation, and lift-off. A transmission electron microscopy (TEM) image of the structure under consideration is shown in Figure 1c in which the relevant excitation positions A, B, and C are indicated. The EELS measurements were performed in a transmission electron microscope (TEM) with a 200 pA probe current and a 300 kV

DOI: 10.1021/acs.nanolett.5b03614
Nano Lett. XXXX, XXX, XXX−XXX

acceleration voltage. The CL measurements were performed in a scanning electron microscope (SEM) with a 800 pA probe current and a 30 kV acceleration voltage (see Supporting Information for more details on fabrication and experimentation). In order to facilitate a proper comparison, the EELS and CL experiments were performed on the same dolmen structure (shown in Figure 1c). As suggested by Guillaume et al. the impact parameter of the electron beam on the dolmen is highly relevant for the resulting EELS and CL response.[39] Figure 2a,b shows EELS and CL spectra measured at locations A and B. At A the electron efficiently drives the longitudinal dipole mode in the top bar. This monomer mode can couple to the antisymmetric dimer mode as observed earlier in optical scattering experiments.[4−6,40,41] The EELS and CL spectra show three peaks at this excitation position, while the CL and EELS spectra for an isolated monomer (gray and black curves in a), taken for reference, only show two clear resonant peaks that correspond to the transverse (λ_0 = 590 nm) and longitudinal (λ_0 = 860 nm) dipole resonances of an individual monomer rod. For excitation at position B we find a clear peak in the CL and EELS spectrum for the bare dimer at 750 nm (gray and black curves in b), which corresponds to the antisymmetric subradiant dimer mode. A similar spectral shape is observed in the EELS and CL spectra for the coupled system excited in region B where the dimer is directly excited. We note that in the EELS spectra there is an additional contribution around λ_0 = 500 nm, which at least partly is due to the vertical electrical dipole mode in the bar. Gold absorbs strongly in this spectral region due to interband transitions so all modes are heavily damped and hence only show up in the EELS measurements.

The extra resonant peak observed at λ_0 = 725 nm in Figure 2a is attributed to the coupling between monomer and dimer. Indeed, in the modal hybridization picture of Figure 1b, the monomer and dimer modes, which each have different energies, will hybridize to form a low-energy bonding mode, with an energy below that of the bare monomer resonance, and a high-energy antibonding mode, with an energy above that of the bare dimer resonance. In this model, the peak at 725 nm is thus attributed to the antibonding mode and the peak at 860 nm corresponds to the bonding mode. Because the dimer and monomer mode are detuned and relatively weakly coupled, the hybridized bonding and antibonding modes are close in frequency to those for the bare monomer and dimer states, where the bonding mode has more monomer character and the antibonding mode has more dimer character.

Even though coupling effects are clearly visible in our measurements, they do not translate into a distinct Fano line shape, a pronounced plasmon-induced transparency window, or a large spectral peak shift between the total extinction (EELS) and radiative response (CL). We envision that increasing the coupling strength by, for instance, going to even smaller particle spacings will make such phenomena more pronounced so that they can be visualized by the combination of EELS and CL spectroscopy at the nanoscale. As the modes at λ_0 = 590 and 725 nm have subradiant character, absorption plays a more important role. This is clearly reflected in the difference in the relative peak amplitudes between EELS and CL. However, these modes are not truly "dark", i.e., invisible in the CL spectrum, as was also suggested in ref 44. The observed EELS and CL lineshapes for A qualitatively match the total extinction (scattering + absorption) and scattering cross section curves for plane-wave excitation with the polarization along the monomer as calculated with FDTD (see Figure S5 in the Supporting Information).

The identification of the dolmen modes and their coupling is corroborated by the spatial maps in Figure 2c for the three resonances. Due to the deep-subwavelength resolution of the electron beam excitation techniques, these maps provide a direct probe of the local field distributions for each mode and give direct visualization of the coupling between the modes. For the λ_0 = 860 nm resonance, a strong excitability is observed at the monomer ends, both for EELS and CL (maps 3 and 6), consistent with the excitation of the bonding dolmen mode in which the dipolar monomer resonance plays an important role. Similarly, at λ_0 = 590 nm, a strong signal is observed for the monomer, both in EELS and CL (maps 1 and 4), corresponding to the transverse dipolar resonance in the monomer, as reflected by the transverse CL/EELS distribution in the monomer. The mode at λ_0 = 725 nm (maps 2 and 5) clearly has more dimer character, although there is still a significant excitation probability at the monomer extremities. The relative excitation efficiency of the antibonding mode compared to the bonding mode does not significantly decline as the beam is moved toward the top of the monomer (this is visualized in Figure S6 in the Supporting Information). From this trend we conclude that the antibonding dolmen mode excitation at A is indeed mediated by the monomer and does not (solely) occur through direct excitation of the dimer with the evanescent electron fields, for which a rapid signal decay is expected away from the dimer. The experimental results shown here have been reproduced on other dolmens with comparable size parameters (see Figure S9 in the Supporting Information).

Thus far we have focused on excitation positions A and B where just one of the dolmen elements is excited by the beam. Next, we investigate the region between the monomer and one of the dimer rods (C), where simultaneous excitation of the dolmen elements occurs. The area of interest is indicated by the multicolored box in the TEM image in Figure 1d. Figure 3a,b shows the CL and EELS spectra when the electron beam moves from the dimer toward the monomer rod (from bottom to top). The colors in the box in Figure 1d are matched to the curve colors of the spectra in (a,b) and indicate the corresponding electron beam position in this direction. The

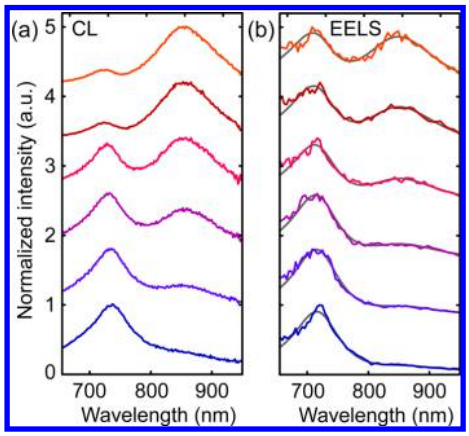

Figure 3. (a,b) CL and EELS spectra moving from the dimer to the top bar (spectra match color code in box in Figure 1d). We transversely average along the width of the box for a better signal-to-noise ratio. The gray curves in (b) are the corresponding numerical fits from the coupled HO model. The spectra are vertically offset for clarity.

DOI: 10.1021/acs.nanolett.5b03614
Nano Lett. XXXX, XXX, XXX−XXX

width of the box (~30 nm) represents the lateral averaging range, which is used to improve the signal-to-noise. This averaging does not significantly alter the observed spectral shape. Clearly, the spectra change completely while the electron beam impact position is varied by only 35 nm, illustrating the nanoscale character of the near-fields in such structures. Close to the dimer, the peak at λ_0 = 725 nm corresponding to the antibonding dolmen mode is dominant. When moving toward the monomer, the peak at 860 nm corresponding to the bonding dolmen mode starts to become stronger; close to the monomer it dominates the spectrum in CL. In the EELS spectra the bonding mode is similar in amplitude to the antibonding mode at this excitation position.

The resonant behavior of coupled plasmonic particles can be described by considering a coupled harmonic mass spring system in which electromagnetic fields act as the driving force. The dolmen particle system response can also be described by a coupled harmonic oscillator (HO) model in which the dipolar monomer mode and antisymmetric dimer mode each represent one oscillator, as was proposed in refs 4 and 6. In those cases plane-wave excitation was considered where the light field exerts a harmonic force on the monomer oscillator. Here, we use an impulse-driven HO model to more accurately describe the transient electron excitation, where the exact electron beam position determines the initial "velocities" that the two oscillators instantaneously receive. The magnitude of these initial velocities can be interpreted as the modal amplitudes of the bare dipolar momomer mode and the antisymmetric dimer mode. The relative sign between the velocities determines whether the two oscillators move in or out-of-phase. To ensure that this two-oscillator description is appropriate we check whether the modes shown in Figure 1b are also dominant for local excitation (see Figure S7 in the Supporting Information for proof; a detailed description of the harmonic oscillator model and fitting procedures are also provided).

This model is most applicable to the EELS data in which the full damping of the system is measured. The resulting spectral curves are plotted together with the data in Figure 3b. The fits match well with the EELS data, showing that one can attain similar lineshapes with such a coupled HO approach. Besides these spectral curves, we also retrieve the initial velocities between the bare dimer and monomer oscillators, which provides a more quantitative insight into the excitation of the two oscillators. In Figure 4 we show the initial oscillator velocity ratio between the bare dimer and monomer mode (v_2/v_1) for different electron beam positions. We notice two trends. First, the dimer velocity v_2 decreases in magnitude compared to v_1 when moving from dimer to monomer. Considering that the plasmonic near-fields roughly follow an exponential decay and that these fields are probed by the point-like electron beam, such a trend is expected. Additionally, we find that for all but one excitation point (closest to the monomer) the velocity ratio is negative, indicating that the oscillators are predominantly driven in antiphase. This is consistent with the notion that the azimuthally symmetric electron beam excitation pins the charges on the dimer and monomer rod[45] (see schematic (1) in Figure 4), thereby favoring excitation of the high-energy antibonding mode. Close to the monomer, direct excitation of the dimer is much weaker ($v_2/v_1 \approx 0$), facilitating excitation of both modes. These results show that by taking advantage of the spatially distinct near-fields and the local character of the electron beam excitation, we

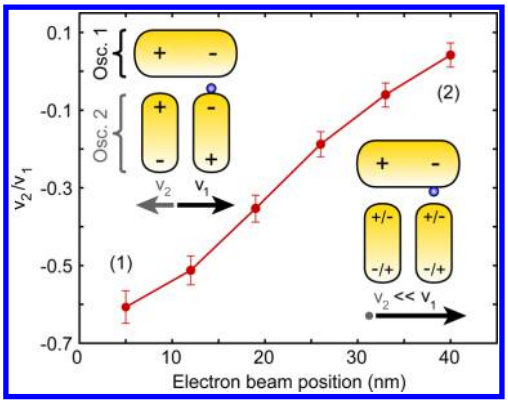

Figure 4. Ratio between initial dimer (v_2) and monomer (v_1) oscillator "velocities" as a function of electron beam position in the gap (where 0 corresponds to excitation at the dimer apex), retrieved from fitting the data in Figure 3b with a coupled harmonic oscillator model. The schematic insets indicate the electron beam positions (blue dot), corresponding charge distributions, and schematic indications of the magnitude/sign of the harmonic oscillator velocities for the leftmost (1) and rightmost (2) data points. The error bars show the 95% confidence interval of the numerical fits.

are able to precisely tune the modal amplitudes providing a new route toward coherent control.

In conclusion, we have demonstrated nanoscale coherent control of a plasmonic dolmen structure by using a focused electron beam. The local electron beam excitation allows for simultaneous excitation of dolmen modes where their relative amplitude can be tuned by precise nanoscale positioning of the beam. We demonstrate that the electron beam excitation of the dolmen can be described by an impulse-driven coupled harmonic oscillator model in which the amplitude of the oscillators is determined by both the electron driving and the near-field coupling between monomer and dimer. These results imply that special care has to be taken when coupling single-emitters to such a metastructure as the exact position of the emitter strongly influences the far-field output and the structure's performance. The novel type of spatial excitation control presented here allows probing and tailoring of the near- and far-field in coupled plasmonic nanostructures with an unprecedented degree of accuracy. As such, it paves the way for a better understanding of modal interaction in the near-field and optimization of structures for specific optical functionality, including radiative decay engineering, sensing, and photochemistry.

■ ASSOCIATED CONTENT

Supporting Information

The Supporting Information is available free of charge on the ACS Publications website at DOI: 10.1021/acs.nanolett.5b03614.

Details on fabrication and experimentation; detailed discussion on the hybridization of modes in the dolmen and FDTD simulations for plane-wave as well as local excitation of the structure; description of the harmonic oscillator model that is used as well as a more elaborate description of the numerical fitting procedure; reproducibility test on three other comparable dolmen structures (PDF)

DOI: 10.1021/acs.nanolett.5b03614
Nano Lett. XXXX, XXX, XXX−XXX

AUTHOR INFORMATION

Corresponding Author

*E-mail: brongersma@stanford.edu.

Present Address

[⊥]Laboratoire de Photonique et Nanostructures, LPN/CNRS, Route de Nozay, 91460 Marcoussis, France

Notes

The authors declare the following competing financial interest(s): A.P. is co-founder and co-owner of Delmic BV, a startup company that develops a commercial product based on the ARCIS cathodoluminescence system that was used in this work.

ACKNOWLEDGMENTS

The work at Stanford was supported by a Multi University Research Initiative (MURI FA9550-12-1-0488) from the AFOSR. This work is also part of the research program of the 'Stichting voor Fundamenteel Onderzoek der Materie' (FOM), which is financially supported by the 'Nederlandse organisatie voor Wetenschappelijk Onderzoek' (NWO). It is also funded by NanoNextNL, a nanotechnology program funded by the Dutch ministry of economic affairs, and the European Research Council (ERC).

REFERENCES

(1) Prodan, E.; Radloff, C.; Halas, N. J.; Nordlander, P. *Science* **2003**, *302*, 419−422.
(2) Kosako, T.; Kadoya, Y.; Hofmann, H. F. *Nat. Photonics* **2010**, *4*, 312−315.
(3) Curto, A. G.; Volpe, G.; Taminiau, T. H.; Kreuzer, M.; Quidant, R.; van Hulst, N. F. *Science* **2010**, *329*, 930−933.
(4) Zhang, S.; Genov, D. A.; Wang, Y.; Liu, M.; Zhang, X. *Phys. Rev. Lett.* **2008**, *101*, 047401.
(5) Verellen, N.; Sonnefraud, Y.; Sobhani, H.; Hao, F.; Moshchalkov, V. V.; Van Dorpe, P.; Nordlander, P.; Maier, S. A. *Nano Lett.* **2009**, *9*, 1663−1667.
(6) Liu, N.; Langguth, L.; Weiss, T.; Kästel, J.; Fleischhauer, M.; Pfau, T.; Giessen, H. *Nat. Mater.* **2009**, *8*, 758−762.
(7) Liu, N.; Weiss, T.; Mesch, M.; Langguth, L.; Eigenthaler, U.; Hirscher, M.; Sönnichsen, C.; Giessen, H. *Nano Lett.* **2010**, *10*, 1103−1107.
(8) Liu, N.; Hentschel, M.; Weiss, T.; Alivisatos, A. P.; Giessen, H. *Science* **2011**, *332*, 1407−1410.
(9) Hentschel, M.; Dregely, D.; Vogelgesang, R.; Giessen, H.; Liu, N. *ACS Nano* **2011**, *5*, 2042−2050.
(10) Sheikholeslami, S. N.; García-Extarri, A.; Dionne, J. A. *Nano Lett.* **2011**, *11*, 3927−3934.
(11) Chang, W. S.; Lassiter, J. B.; Swanglap, P.; Sobhani, H.; Khatua, S.; Nordlander, P.; Halas, N. J.; Link, S. *Nano Lett.* **2012**, *12*, 4977−4982.
(12) Frimmer, M.; Coenen, T.; Koenderink, A. F. *Phys. Rev. Lett.* **2012**, *108*, 077404.
(13) Rodriguez, S. R. K.; Murai, S.; Verschuuren, M. A.; Gómez Rivas, J. *Phys. Rev. Lett.* **2012**, *109*, 166803.
(14) Wu, C.; Khanikaev, A. B.; Adato, R.; Arju, N.; Yanik, A. A.; Altug, H.; Shvets, G. *Nat. Mater.* **2011**, *11*, 69−75.
(15) Fang, Z.; Wang, Y.; Liu, Z.; Schlather, A.; Ajayan, P. M.; Koppens, F. H. L.; Nordlander, P.; Halas, N. J. *ACS Nano* **2012**, *6*, 10222−10228.
(16) Gallinet, B.; Martin, O. J. F. *ACS Nano* **2013**, *7*, 6978−6987.
(17) Hokari, R.; Kanamori, Y.; Hane, K. *Opt. Express* **2014**, *22*, 3526−3537.
(18) Stockman, M. I.; Faleev, S. V.; Bergman, D. *Phys. Rev. Lett.* **2002**, *88*, 067402.
(19) Brinks, D.; Castro-Lopez, M.; Hildner, R.; van Hulst, N. F. *Proc. Natl. Acad. Sci. U. S. A.* **2013**, *110*, 18386−18390.
(20) Gjonaj, B.; Aulbach, J.; Johnson, P. M.; Mosk, A. P.; Kuipers, L.; Lagendijk, A. *Nat. Photonics* **2011**, *5*, 360−363.
(21) Sukharev, M.; Seideman, T. *Nano Lett.* **2006**, *6*, 715−719.
(22) Zeuner, F.; Muldarisnur, M.; Hildebrandt, A. F. J.; Zentgraf, T. *Nano Lett.* **2015**, *15*, 4189−4193.
(23) Coenen, T.; Vesseur, E. J. R.; Polman, A.; Koenderink, A. F. *Nano Lett.* **2011**, *11*, 3779−3784.
(24) Yamamoto, N.; Ohtani, S.; García de Abajo, F. J. *Nano Lett.* **2011**, *11*, 91−95.
(25) Denisyuk, A. I.; Adamo, G.; MacDonald, K. F.; Edgar, J.; Arnold, M. D.; Myroshnychenko, V.; Ford, J.; García de Abajo, F. J.; Zheludev, N. I. *Nano Lett.* **2010**, *10*, 3250−3252.
(26) Lassiter, J. B.; Sobhani, H.; Knight, M. W.; Mielczarek, W. S.; Nordlander, P.; Halas, N. J. *Nano Lett.* **2012**, *12*, 1058−1062.
(27) Fung, K. H.; Kumar, A.; Fang, N. X. *Phys. Rev. B: Condens. Matter Mater. Phys.* **2014**, *89*, 045408.
(28) Koh, A. L.; Fernández-Domínguez, A.; McComb, D.; Maier, S.; Yang, J. *Nano Lett.* **2011**, *11*, 1323−1330.
(29) Alber, I.; Sigle, W.; Müller, S.; Neumann, R.; Picht, O.; Rauber, M.; van Aken, P. A.; Toimil-Molares, M. A. *ACS Nano* **2011**, *5*, 9845−9853.
(30) Scholl, J. A.; García-Etxarri, A.; Koh, A. L.; Dionne, J. A. *Nano Lett.* **2013**, *13*, 564−569.
(31) Barrow, S.; Rossouw, D.; Funston, A. M.; Botton, G. A.; Mulvaney, P. *Nano Lett.* **2014**, *14*, 3799−3808.
(32) Collins, S. M.; Nicoletti, O.; Rossouw, D.; Ostasevicius, T.; Midgley, P. A. *Phys. Rev. B: Condens. Matter Mater. Phys.* **2014**, *90*, 155419.
(33) Tan, S. F.; Wu, L.; Yang, J. K. W.; Bai, P.; Bosman, M.; Nijhuis, C. A. *Science* **2014**, *343*, 1496−1499.
(34) García de Abajo, F. J. *Rev. Mod. Phys.* **2010**, *82*, 209−275.
(35) Sapienza, R.; Coenen, T.; Renger, J.; Kuttge, M.; van Hulst, N. F.; Polman, A. *Nat. Mater.* **2012**, *11*, 781−787.
(36) Myroshnychenko, V.; Nelayah, J.; Adamo, G.; Geuquet, N.; Rodríguez-Fernández, J.; Pastoriza-Santos, I.; MacDonald, K. F.; Henrard, L.; Liz-Marzán, L. M.; Zheludev, N. I.; Kociak, M.; García de Abajo, F. J. *Nano Lett.* **2012**, *12*, 4172−4180.
(37) Kociak, M.; Stéphan, O. *Chem. Soc. Rev.* **2014**, *43*, 3865−3883.
(38) Losquin, A.; Zagonel, L. F.; Myroshnychenko, V.; Rodríguez-González, B.; Tencé, M.; Scarabelli, L.; Förstner, J.; Liz-Marzán, L. M.; García de Abajo, F. J.; Stéphan, O.; Kociak, M. *Nano Lett.* **2015**, *15*, 1229−1237.
(39) Guillaume, S. O.; Geuquet, N.; Henrard, L. *Proc. SPIE* **2011**, *8096*, 80962E.
(40) Ye, Z.; Zhang, S.; Wang, Y.; Park, Y.; Zentgraf, T.; Bartal, G.; Yin, X.; Zhang, X. *Phys. Rev. B: Condens. Matter Mater. Phys.* **2012**, *86*, 155148.
(41) Forestiere, C.; Dal Negro, L.; Miano, G. *Phys. Rev. B: Condens. Matter Mater. Phys.* **2013**, *88*, 155411.
(42) Abasahl, B.; Santschi, C.; Martin, O. J. F. *ACS Photonics* **2014**, *1*, 403−407.
(43) Yan, C.; Martin, O. J. F. *ACS Nano* **2014**, *8*, 11860−11868.
(44) Bernal Arango, F.; Coenen, T.; Koenderink, A. F. *ACS Photonics* **2014**, *1*, 444−453.
(45) Bigelow, N. W.; Vaschillo, J. P.; Camden; Masiello, D. J. *ACS Nano* **2013**, *7*, 4511−4519.

DOI: 10.1021/acs.nanolett.5b03614
Nano Lett. XXXX, XXX, XXX−XXX